Test of Causal Nonlinear Quantum Mechanics by Ramsey Interferometry with a Trapped Ion

Joseph Broz, Bingran You, Sumanta Khan, and Hartmut Häffner
Department of Physics, University of California, Berkeley, California 94720, USA
and Challenge Institute for Quantum Computation, University of California, Berkeley, California 94720, USA

David E. Kaplan and Surjeet Rajendran
Department of Physics and Astronomy, The Johns Hopkins University, Baltimore, Maryland 21218, USA

(Received 27 June 2022; accepted 6 April 2023; published 15 May 2023)

Quantum mechanics requires the time evolution of the wave function to be linear. While this feature has been associated with the preservation of causality, a consistent causal nonlinear theory was recently developed. Interestingly, this theory is unavoidably sensitive to the full physical spread of the wave function, rendering existing experimental tests for nonlinearities inapplicable. Here, using well-controlled motional superpositions of a trapped ion, we set a stringent limit of 5.4×10^{-12} on the magnitude of the unitless scaling factor $\tilde{\epsilon}_\gamma$ for the predicted causal nonlinear perturbation.

DOI: 10.1103/PhysRevLett.130.200201

Introduction.—Quantum mechanics (QM) is central to our understanding of nature. Its principles are used to predict phenomena ranging from the microscopic world of atoms and nuclei, to the mesoscopic world of solids and materials, and the macroscopic behavior of the cosmos. Given its central importance to all branches of physics, it is important to test its foundations. One of the key foundations of QM is that the time evolution of a quantum system is described by a linear equation of motion. This axiom underpins a number of important results in QM [1] including the no-cloning theorem [2].

Given that linearity is an approximation in every other known physical theory, why should linearity be an absolute requirement of QM? There have been many theoretical suggestions [3–6] for incorporating nonlinear evolution in single particle QM. But QM needs to be able to describe multiple particles that can exist together in an arbitrarily complicated entangled state. Naive generalizations of [3–6] to such states generally lead to violations of causality (i.e., instantaneous communication of information) [7–9], contributing to a widespread belief that linearity is necessary for causality [10]. However, as first pointed out by Polchinski [9], causal nonlinear quantum mechanical (NLQM) evolution of multiparticle states is possible if the nonlinear terms in the Schrödinger equation are restricted to a specific form.

Recently, Kaplan and Rajendran [11], building on earlier work by Kibble [12], have developed a systematic approach for incorporating causal nonlinear evolution into quantum field theory (QFT). The introduction of nonlinearities directly into QFT as opposed to the single particle Schrödinger equation is motivated by the fact that QFT is the natural framework to describe the causal evolution of multiparticle states. And it was shown in [11] that the seemingly unmotivated [13] nonlinear structure demanded by [9] for multiparticle states was a direct physical consequence of QFT.

Importantly, [11] and [9] recognized that, unlike linear QM where the physical spread of the wave function is irrelevant for QM observables such as energy levels of quantum systems, any causal NLQM theory is highly susceptible to the physical spread of the wave function. This aspect of NLQM was not appreciated in prior experimental work [14–19] and thus the bounds on causal NLQM theories imposed by these experiments are quite weak [11]. In light of the existence of possible causal NLQM theories and the weak nature of these bounds, it is important to robustly experimentally test parametrized nonlinear deviations from QM. These tests are particularly important since deviations away from linear QM may open new doors to solving long-standing problems in physics such as the black hole information problem while potentially enabling a variety of new technological possibilities [11].

The basic approach of [11] is to start with a given QFT and introduce nonlinearities by shifting bosonic field operators by a small amount proportional to the expectation value of the field operator acting on the full quantum state. When applied to single particle systems, the procedure yields a nonlinear Schrödinger equation. For example, the time evolution of a single particle with charge q and Hamiltonian H is described in this theory by

$$i\hbar\partial_t\Psi(t,\mathbf{x}) = \left(H + \tilde{\epsilon}_\gamma \frac{q^2}{4\pi\epsilon_0}\int d^4\mathbf{x}_1 |\Psi(t_1,\mathbf{x}_1)|^2 G_r(t,\mathbf{x};t_1,\mathbf{x}_1)\right) \times \Psi(t,\mathbf{x}), \quad (1)$$

 © 2023 American Physical Society

where $\tilde{\epsilon}_\gamma$ is a small unitless parameter scaling the nonlinearity of the theory [20] and G_r is the relativistic retarded Green's function from the spacetime coordinates $(t_1, \mathbf{x}_1)$ to $(t, \mathbf{x})$. G_r naturally appears in this expression from the underlying QFT derivation and enforces causality. The new term added to the Hamiltonian in Eq. (1) admits the simple interpretation of a classical Coulomb potential causally sourced by the quantum probability distribution of the particle's position.

One might expect that strong bounds set from previous searches for NLQM [14–19] would limit this theory. But this expectation turns out to be false for the following fundamental reason. The tests performed by [14–19] are on energy levels of various bound states. In linear QM, the level structure is independent of the center of mass spread of the bound state wave function. This is not true in causal NLQM where nonlinear effects alter time evolution via the position space wave function as in Eq. (1). These effects are highly suppressed if the center of mass wave function is spread out.

To illustrate this point, it is helpful to take the nonrelativistic limit of Eq. (1). When $\|H\|/\hbar \ll c/|\mathbf{x}_1 - \mathbf{x}|$ the nonlinear Schrödinger equation becomes

$$i\hbar\partial_t\Psi(t,\mathbf{x}) = \left(H + \tilde{\epsilon}_\gamma \frac{q^2}{4\pi\epsilon_0}\int d^3\mathbf{x}_1 \frac{|\Psi(t,\mathbf{x}_1)|^2}{|\mathbf{x}_1 - \mathbf{x}|}\right)\Psi(t,\mathbf{x}). \tag{2}$$

Here one can see that the denominator of the integrand scales with the full position-space spread of the wave function, damping the perturbation accordingly. This is a simple consequence of the Coulomb potential that sources the nonlinearity, but the implication is that any sensitive test based on standard atomic or nuclear spectroscopy must also pin down the test system's center of mass motion to a dimension comparable to the spread of the internal degrees of freedom—particularly for neutral test particles. This condition was not well satisfied in previous tests for NLQM [14–19], but by requiring the nonlinear correction to be smaller than the uncertainty in recent Lamb shift measurements of hydrogen, Kaplan and Rajendran have set a modest bound of $|\tilde{\epsilon}_\gamma| \lessapprox 10^{-4}$, giving a sense for the limitations of atomic spectroscopy [11].

For a more precise test, one can take advantage of the net charge of a trapped ion by performing Ramsey spectroscopy [21] on a superposition of the Fock states $|n\rangle$ describing one of its harmonic vibrational modes [11]. The state $|\psi(t=0)\rangle = \alpha_n|n\rangle + \alpha_m|m\rangle$ can be prepared and then allowed to freely evolve for an interrogation time τ. The Coulomb field sourced by the position-space expectation value of $|\psi\rangle$ interacts differently with the two branches of the wave function leading to an energy shift and thus measurable accumulated phase difference between them [22]. If $|n\rangle$ is chosen to be more spatially localized than $|m\rangle$, one can increase (decrease) the strength of the nonlinearity by increasing (decreasing) the relative population $|\alpha_n|^2$ of $|n\rangle$.

For $n = 0$ and $m = 1$ this already results in a significant effect. Replacing H in Eq. (2) with the Hamiltonian for a three-dimensional, isotropic harmonic oscillator [23] and assuming the vibrational modes in the transverse plane remain in their ground state, the phase difference accumulated between the ground and first excited state of the superposition after a time τ is given by

$$\phi_{\mathrm{NL}}(\tau;\{\alpha_i\}) = \tilde{\epsilon}_\gamma \frac{10\alpha_0^2 + \alpha_1^2}{30\sqrt{2\pi}\hbar}\frac{e^2}{4\pi\epsilon_0 x_0}\tau, \tag{3}$$

where the α_i are assumed to be real and $x_0 = \sqrt{\hbar/m\nu}$ is the characteristic length scale of a harmonic oscillator with mass m and natural frequency ν. Note that the state dependence of ϕ_{NL}, i.e., its dependence on the weight of the energy eigenstates via α_i, is a characteristic nonlinear effect, which has no analog in the linear theory. For an ion localized to $x_0 = 10$ nm, a phase of up to order $10^{10} \times \tilde{\epsilon}_\gamma$ is accumulated for every millisecond of interrogation time. In this Letter we perform such a Ramsey experiment designed to maximize the signal ϕ_{NL} and thus tighten the bound on $\tilde{\epsilon}_\gamma$ by 8 orders of magnitude relative to the current best estimate.

Experimental implementation.—Experiments were performed using a single $^{40}Ca^+$ ion confined inside of a radio-frequency (rf) Paul trap in a parameter regime where the center of mass motion is well modeled as a three-dimensional anisotropic harmonic oscillator [Fig. 1(a)] with vibrational frequencies $\nu_x \approx 2\pi \times 1.01$, $\nu_y \approx 2\pi \times 2.52$, and $\nu_z \approx 2\pi \times 2.79$ MHz.

The ion's internal state is manipulated by shining resonant laser light on various electronic transitions [Fig. 1(b)]. The short-lived $4^2S_{1/2} \leftrightarrow 4^2P_{1/2}$ and $3^2D_{5/2} \leftrightarrow 4^2P_{3/2}$ dipole transitions are used for entropy-altering operations like cooling and measurement. Measurement, in particular, is performed via the electron shelving method on $4^2S_{1/2} \leftrightarrow 4^2P_{1/2}$ and allows us to determine the population of the $4^2S_{1/2}$ manifold [24]. For coherent operations, narrow band light at 729 nm is used to couple the $|4^2S_{1/2}, m_J = -1/2\rangle$ and $|3^2D_{5/2}, m_J = -1/2\rangle$ states, whose degeneracy is broken with a static magnetic field of $B \approx 4$ G. We call this our qubit transition and reference it as $|S\rangle \leftrightarrow |D\rangle$.

To prepare the ion in a well-defined state, we first cool its temperature to several hundred microkelvins using Doppler cooling and then optically pump its electronic state into $|S\rangle$. Afterward, resolved sideband cooling is applied along the x direction, driving the axial vibrational mode into its ground state with high probability [25]. Once this process is complete, the ion is measured to be in the state $|S, n_x = 0\rangle$ with a confidence greater than 99%, where n_x refers to the phonon number of the vibrational mode along the x direction. The two transverse vibrational modes are left in thermal states

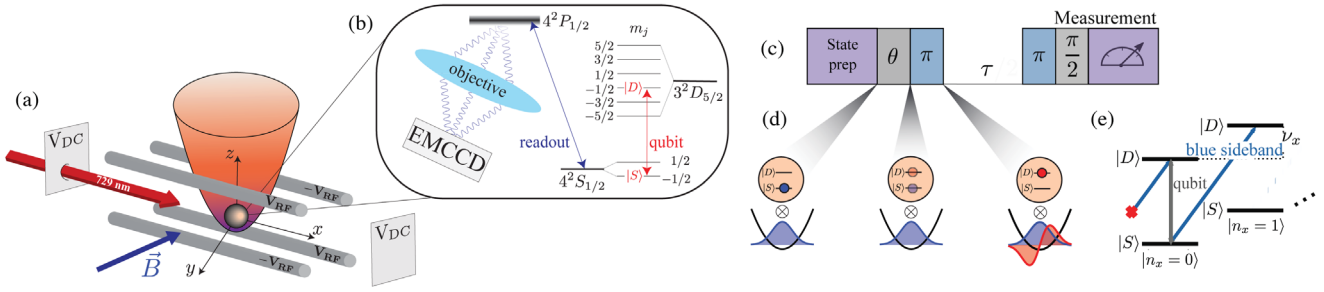

FIG. 1. Experimental implementation. (a) A $^{40}Ca^+$ ion is trapped using a combination of rf and dc electric fields. In a time-averaged sense, the confinement is well modeled by a three-dimensional harmonic potential. (b) Motion along the x direction is excited by resonantly coupling to the internal electronic Zeeman sublevels of the $4^2S_{1/2} \leftrightarrow 3^2D_{5/2}$ transition using narrow band light near 729 nm. The degeneracy of the Zeeman states is broken through application of a strong magnetic field of ≈4 G. Measurement is performed by scattering photons of the short-lived $4^2S_{1/2} \leftrightarrow 4^2P_{1/2}$, which are then focused onto an EMCCD camera. (c) The experimental pulse sequence. Pulses that address the qubit are colored gray and those that address the blue sideband, blue. After preparing the state $|S,0\rangle$, the first pair of pulses is used to generate the state $|\psi(t=0)\rangle = |D\rangle(\alpha_0|0\rangle + \alpha_1|1\rangle)$. This is then allowed to freely evolve for a time τ, accumulating a relative phase of $\Phi(\tau)$, which is sensitive to the proposed causal nonlinear perturbation. Afterward, the information is mapped onto the qubit with a blue sideband pulse and then the expectation value of the Pauli spin operator $\cos(\xi_L)\sigma_x + \sin(\xi_L)\sigma_y$ is measured. (d) An illustration of the two-step process for generating the state $|\psi(t=0)\rangle$, as described in more detail in the main text. The key feature is the fact that the state $|D,0\rangle$ is transparent to the resonant blue sideband drive as illustrated in (e). This allows us to map an arbitrary qubit state onto the ground and first excited state of the vibrational mode.

with mean phonon occupations determined by the Doppler limit of $\langle n_{y,z}\rangle \approx 3$. These modes remain separated from the $|S,n_x\rangle$ state and so we ignore them in what follows except for taking into account the additional spread of the wave function in position space to determine the nonlinearity in Eqs. (2) and (3).

In order to create the desired superposition state, we use laser light resonant with a motional sideband of the qubit transition. From the ion's perspective, a laser pointing along one of its vibrational axes will appear to be phase modulated by motion along that direction. By detuning the laser from the qubit frequency by an amount equal to $+\nu_x$, this effect can be used to couple the states $|S,n\rangle \leftrightarrow |D,n+1\rangle$, which we refer to as blue sideband transitions [Fig. 1(e)] [26]. The energy of the blue sideband transitions is already sensitive to the nonlinear perturbation and, in principle, can be used for our Ramsey experiment. But the electronic states are first-order sensitive to ambient magnetic field fluctuations leading to a coherence time an order of magnitude less than that of the vibrational mode—unnecessarily limiting the Ramsey interrogation time.

So, instead we first map the desired Ramsey superposition onto the ion's internal states by resonantly driving the qubit transition for a fixed duration, generating the state $(\alpha_1|S\rangle + \alpha_0|D\rangle)|0\rangle$, in an appropriate rotating frame. Here $\alpha_0 = \sin(\theta/2)$, $\alpha_1 = \cos(\theta/2)$ and the value of θ is controlled by adjusting the intensity of the addressing laser. Next, we drive a blue sideband π pulse that nominally transfers all of the population from $|S,0\rangle$ to $|D,1\rangle$ but leaves the population in $|D,0\rangle$ untouched [Figs. 1(d)–1(e)]. Together, these operations result in the separated state $|\psi(t=0)\rangle = |D\rangle(\alpha_0|0\rangle + \alpha_1|1\rangle)$, where the qubit state information has been written onto the vibrational mode [22].

Once the state $|\psi\rangle$ has been prepared, it is allowed to evolve freely for a time τ so that a relative phase $\Phi(\tau;\theta)$ is accumulated and $|\psi(\tau)\rangle = |D\rangle(\alpha_0|0\rangle + e^{i\Phi(\tau,\theta)}\alpha_1|1\rangle)$. To extract this phase, we repeat the steps used to generate $|\psi(0)\rangle$ in a time-reversed order (with the value of θ now fixed at $\pi/2$ where the signal is maximized) and then measure $|D\rangle$, which will be occupied with a probability of

$$P(\tau) = B - \frac{A(\tau)}{2}\cos[\Phi(\tau;\theta) + \xi_L], \tag{4}$$

where $0 \le A(\tau) \le 1$ is the signal contrast which will generally be less than one when $\theta \neq \pi/2$, $B \approx 1/2$ is an offset whose precise value is sensitive to errors in state preparation or measurement, and ξ_L is the laser phase of the final qubit $\pi/2$-pulse relative to the initial θ pulse. Since $P(\tau)$ is an expectation value, a single estimate is obtained by repeating the experiment 200 times, which is large enough that the propagation of the quantum projection noise (QPN) converges when inverting Eq. (4). The full pulse sequence is illustrated in Fig. 1(c).

In order to gauge the performance of the Ramsey experiment, we conduct a test experiment where we apply a detuning Δ from resonance of several kHz to the first blue sideband pulse. In the rotating frame, this breaks the degeneracy of $|0\rangle$ and $|1\rangle$ leading to a phase of $\Phi(\tau) = \Delta\tau$ and, thus, sinusoidal oscillations of $P(\tau)$. The result is plotted in Fig. 2(a), where one can see that the signal contrast $A(\tau)$ exhibits a clear time dependence due to zero-mean noise effects beyond the simple model described in Eq. (4).

The dominant source of this noise is found to be a Markovian heating of the vibrational mode caused by

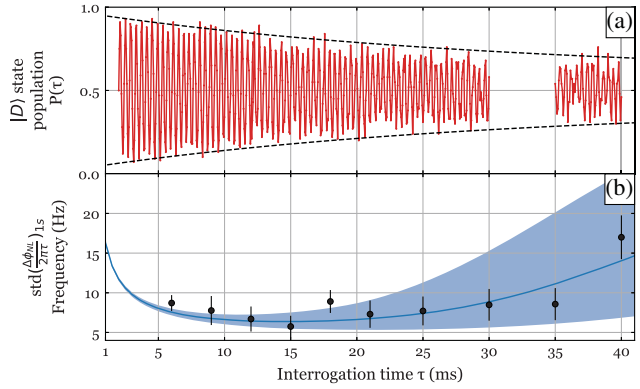

FIG. 2. Experimental performance.—(a) Measured $P(\tau)$, as described by Eq. (4) (red). The black dashed line is the predicted decay envelope taking into account only heating of the vibrational mode at a rate of 10 quanta/s. The reasonable agreement between the predicted and measured decay suggests that the Ramsey signal contrast is dominated by this heating process. (b) The black circles represent the sample standard deviation from repeated measurements of $\Delta\phi_{\mathrm{NL}}(\tau)$ taken at various interrogation times and normalized to an integration time of 1 s. The blue shaded region bounds the simulated predictions assuming only QPN and a heating rate between 7 and 13 quanta/s (lower and upper edge of the region, respectively). The dark blue line corresponds to 10 quanta/s.

ambient electric field fluctuations at the position of the ion and, perhaps, high frequency noise on the trapping potential [27]. This means that during free evolution, the vibrational mode may spontaneously absorb a phonon from its environment with a probability that grows linearly in time. When n phonons are absorbed, the state of the system after the final blue sideband pulse will be $|S\rangle(\alpha_0|n\rangle + \alpha_1|n+1\rangle)$ and the result of the final $\pi/2$ pulse, regardless of Φ, will be a symmetric distribution of $\{|S\rangle, |D\rangle\}$—diminishing the averaged signal contrast. The dashed line in Fig. 2(a) is a simulated decay envelope computed assuming only this heating process as characterized by the heating rate $\dot{\bar{n}} \approx 10$ quanta/s, independently measured by monitoring the red sideband [26]. The good agreement between the simulated and measured decay validates our earlier claim that the contrast is limited by environmental heating.

For a precise determination of the nonlinearity it is most convenient to estimate $\Phi(\tau)$ at a fixed τ. But since A, B, and Φ are all empirical quantities, inverting Eq. (4) requires at least three independent measurements. We obtain these by repeating the experiment for three different values of ξ_L spaced by ninety degrees such that $\xi_L^{(3)} = \xi_L^{(2)} + \pi/2 = \xi_L^{(1)} + \pi$. The targeted value of $\xi_L^{(1)}$ is chosen to minimize the standard deviation of $\Phi(\tau)$:

$$|\delta\Phi(\tau)| = \sqrt{\sum_i \left(\frac{\partial\Phi}{\partial \mathrm{P}_i}\delta \mathrm{P}_i\right)^2}, \tag{5}$$

which occurs when $\Phi(\tau) + \xi_L^{(1)} = \pi/2$. Here P_i is the population measurement associated with $\xi_L^{(i)}$ and δP_i is its standard deviation, nominally dominated by QPN.

A single measurement of $\Phi(\tau)$ contains the nonlinear signature $\phi_{\mathrm{NL}}(\tau)$, as described by Eq. (3), but also includes information about the detuning Δ of the blue sideband pulses from resonance and any ac Stark shifts that occur during state preparation and readout. Explicitly: $\Phi(\tau;\theta) = \phi_{\mathrm{NL}}(\tau;\theta) + \Delta\tau + \phi_{SS}$, where ϕ_{SS} is the phase imprinted by the Stark shifts. Ideally, the frequency of the blue sideband pulses are calibrated such that $\Delta = 0$, but slow drifts of the trapping potential on a timescale that is long relative to the Ramsey interrogation time generally cause this condition to be violated. Likewise, Stark shifts incurred while driving the blue sideband cause a phase offset. But importantly, both Δ and ϕ_{SS} are independent of θ meaning that we can obtain an unbiased estimate of the nonlinearity by repeating the measurement for two different values of θ and taking their difference:

$$\begin{aligned}\Delta\phi_{\mathrm{NL}}(\tau;\{\theta_i\}) &= \Phi(\tau;\theta_1) - \Phi(\tau;\theta_2) \\ &= \phi_{\mathrm{NL}}(\tau;\theta_1) - \phi_{\mathrm{NL}}(\tau;\theta_2).\end{aligned} \tag{6}$$

We choose θ_1 and θ_2 such that the ground state population of $|\psi(t=0)\rangle$ is 0.2 and 0.8, respectively. We also verify that there is no phase difference due to the Stark shift for both preparation sequences.

The nonlinear signal $\Delta\phi_{\mathrm{NL}}$ grows linearly with interrogation time τ. But this effect must contend with the contrast decay and QPN, both of which increase the uncertainty of the signal [Eq. (5)] and both of which favor shorter, more frequent measurements [28]. The combination of these effects results in an optimal interrogation time, which we determine experimentally by measuring $\Delta\phi_{\mathrm{NL}}(\tau)$ at various τ and computing the sample standard deviation. These results are normalized to an integration time of 1 s and plotted in Fig. 2(b). The blue-shaded region is a corresponding simulation that assumes only QPN and vibrational heating bounded by $7 \leq \dot{\bar{n}} \leq 13$ quanta/s. Based on this data, we fix $\tau = 15$ ms.

To determine a more rigorous bound on $\tilde{\epsilon}_\gamma$ we repeat the measurement of $\Delta\phi_{\mathrm{NL}}(\tau = 15\ \mathrm{ms})$ many times. Before each ϕ_{NL} measurement, we independently measure the initial qubit excitation to determine the precise values of θ_i which may change slightly over time due to intensity drifts of the addressing light. We also perform a preliminary three-point Ramsey measurement with the population of $|0\rangle$ set to 0.5 to produce a maximum signal that we use to optimally bias $\xi_L^{(1)}$. Next, we perform 1200 measurements of the Ramsey signal, 200 for each of the 3 Ramsey points for θ_1 and θ_2. The ordering of these experiments is randomized so as to avoid a bias due to drifts in $\Phi(\tau)$. From this data we compute $\Delta\phi_{\mathrm{NL}}$, the average contrast A of the two runs and the average offset B. For a single day of

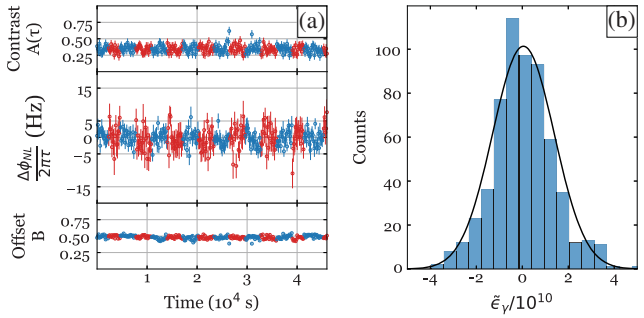

FIG. 3. Results. (a) (top to bottom) The measured contrast, frequency and offset over a full day of data collection. The blue circles represent data taken at an interrogation time of 15 ms and the red circles were taken at a time of 15 ms divided by the golden ratio (≈9.3 ms). (b) The distribution of $\tilde{\epsilon}_\gamma$ estimated from the data. The mean value is $5 \pm 5.4 \times 10^{-12}$. The black curve is a Gaussian fit to the distribution.

data, this is plotted in Fig. 3(a). The blue dots show data taken at $\tau = 15$ ms. The red dots show data taken at 15 ms divided by the golden ratio $(1+\sqrt{5})/2 \approx 9.27$ ms, which does not improve the estimate of the nonlinearity but allows us to rule out the remote possibility that $\Delta\phi_{\mathrm{NL}}(\tau = 15\ \mathrm{ms})$ modulo 2π vanishes even though the perturbation is not small.

The distribution of $\tilde{\epsilon}_\gamma$ computed from the measured values of $\Delta\phi_{\mathrm{NL}}(\tau = 15\ \mathrm{ms})$ and θ_i is shown in Fig. 3(b). The black curve is a Gaussian fit. The mean value is determined to be $5 \pm 5.4 \times 10^{-12}$ where the reported uncertainty corresponds to 1 standard deviation. The average uncertainty of the individual measurements computed using standard propagation of error when solving the system of equations Eqs. (5), (6) and assuming only QPN is found to be 7.7×10^{-11}, which is in good agreement with the sample standard deviation 8.2×10^{-11}.

In summary, we have improved the bound on causal NLQM from $|\tilde{\epsilon}_\gamma| \lessapprox 10^{-4}$ to $|\tilde{\epsilon}_\gamma| \lessapprox 5.4 \times 10^{-12}$ while illustrating the challenges and highlighting a generalizable solution for designing sensitive probes of causal NLQM with a simple and easy-to-understand experiment. Better sensitivity could be achieved via technical improvements, e.g., longer averaging times, longer coherence times, higher mass atoms, larger trapping potentials or superpositions of the ground and higher order Fock states. In addition, one could use vibrational Fock state superpositions of the center-of-mass mode of many identical ions in the same trap [29] and/or more sophisticated quantum measurement protocols such as a superposition of squeezed states.

As a final note, we emphasize that though we probe for nonlinearities sourced from electromagnetic fields, the framework outlined in [11] is quite general and permits the incorporation of nonlinearities in any interacting field theory—including gravitation. Thus, the framework could potentially be extended to gravitational collapse models where gravitational interactions are believed to cause a quantum state to collapse when it evolves toward a macroscopic superposition. While trapped ion systems are ill suited for probes of gravitational interactions, this work may serve to inspire future searches of nonlinearities sourced from gravity or one of the other forces.

J. B., S. K., and H. H. acknowledge funding by the U.S. Department of Energy, Office of Science, Office of Basic Energy Sciences under Awards No. DE-SC0019376 and No. DE-SC0023277. S. R. and D. K. are supported in part by the U.S. National Science Foundation (NSF) under Grant No. PHY-1818899. This work was supported by the U.S. Department of Energy (DOE), Office of Science, National Quantum Information Science Research Centers, Superconducting Quantum Materials and Systems Center (SQMS) under Contract No. DE-AC02-07CH11359. S. R. is also supported by the DOE under a QuantISED grant for MAGIS, and the Simons Investigator Grant No. 827042.

Note added.—Recently, we became aware of related work [30].

[1] E. P. Wigner, Ann. Math. **40**, 149 (1939).
[2] W. K. Wootters and W. H. Zurek, Nature (London) **299**, 802 (1982).
[3] I. Bialynicki-Birula and J. Mycielski, Ann. Phys. (N.Y.) **100**, 62 (1976).
[4] S. Weinberg, Phys. Rev. Lett. **62**, 485 (1989).
[5] S. Weinberg, Ann. Phys. (N.Y.) **194**, 336 (1989).
[6] H.-D. Doebner and G. A. Goldin, Phys. Lett. **162A**, 397 (1992).
[7] N. Gisin, Phys. Lett. **143A**, 1 (1990).
[8] N. Gisin, Helv. Phys. Acta **62**, 363 (1989).
[9] J. Polchinski, Phys. Rev. Lett. **66**, 397 (1991).
[10] A. Bassi and K. Hejazi, Eur. J. Phys. **36**, 055027 (2015).
[11] D. E. Kaplan and S. Rajendran, Phys. Rev. D **105**, 055002 (2022).
[12] T. W. B. Kibble, Commun. Math. Phys. **64**, 73 (1978).
[13] A. Kapustin, arXiv:1303.6917.
[14] C. G. Shull, D. K. Atwood, J. Arthur, and M. A. Horne, Phys. Rev. Lett. **44**, 765 (1980).
[15] R. Gahler, A. G. Klein, and A. Zeilinger, Phys. Rev. A **23**, 1611 (1981).
[16] J. J. Bollinger, D. J. Heinzen, W. M. Itano, S. L. Gilbert, and D. J. Wineland, Phys. Rev. Lett. **63**, 1031 (1989).
[17] T. E. Chupp and R. J. Hoare, Phys. Rev. Lett. **64**, 2261 (1990).
[18] R. L. Walsworth, I. F. Silvera, E. M. Mattison, and R. F. C. Vessot, Phys. Rev. Lett. **64**, 2599 (1990).
[19] P. K. Majumder, B. J. Venema, S. K. Lamoreaux, B. R. Heckel, and E. N. Fortson, Phys. Rev. Lett. **65**, 2931 (1990).
[20] The γ subscript specifies that this perturbation is specific to electromagnetic fields. The causal theory is field-dependent and does not explicitly require that the scaling of the perturbation be the same for self-interactions mediated by different quantum field theories.

[21] N. Ramsey, in *Molecular Beams* (Oxford University Press, Oxford, England, UK, 1956).
[22] F. Schmidt-Kaler, S. Gulde, M. Riebe, T. Deuschle, A. Kreuter, G. Lancaster, C. Becher, J. Eschner, H. H. ffner, and R. Blatt, J. Phys. B **36**, 623 (2003).
[23] For an anisotropic potential, Eq. (3) will incur an $\mathcal{O}(\tilde{\epsilon}_\gamma)$ correction, which is taken into account for the final reported value.
[24] W. Nagourney, J. Sandberg, and H. Dehmelt, Phys. Rev. Lett. **56**, 2797 (1986).
[25] F. Diedrich, J. C. Bergquist, W. M. Itano, and D. J. Wineland, Phys. Rev. Lett. **62**, 403 (1989).
[26] D. Leibfried, R. Blatt, C. Monroe, and D. Wineland, Rev. Mod. Phys. **75**, 281 (2003).
[27] S. Schneider and G. J. Milburn, Phys. Rev. A **59**, 3766 (1999).
[28] S. F. Huelga, C. Macchiavello, T. Pellizzari, A. K. Ekert, M. B. Plenio, and J. I. Cirac, Phys. Rev. Lett. **79**, 3865 (1997).
[29] This effectively increases the mass of the vibrational mode as well as the number of independent measurements.
[30] M. Polkovnikov, A. V. Gramolin, D. E. Kaplan, S. Rajendran, and A. O. Sushkov, Phys. Rev. Lett. **130**, 040202 (2023).